# Fringing Field Formulas and Winding Loss Due to an Air Gap

Waseem A. Roshen

Physics Department, The Ohio State University, Hilliard, OH 43026 USA

**The paper describes a simple treatment for the fringing fields of an air gap in the core of a magnetic component such as an inductor or a transformer. It verifies the derived analytical formulas for the fields by using numerical (finite-element) calculations. It then applies these formulas to the calculation of high-frequency eddy-current losses for two types of winding arrangements, both of which employ thin rectangular conductors. The rectangular conductors are commonly used in flex circuit windings, printed circuit windings, and thin-film windings. The two types of winding configurations are flat and barrel wound. Each behaves in a different way as a function of the position of the conductor.**

***Index Terms*—Air gap, fringing field, high frequency, inductor, motors, power conditioning, power conversion, power electronics, transformer, winding loss.**

## I. Introduction

In MANY high-performance power electronics applications, the design of the magnetic components, such as inductors and transformers, is the most important factor since it affects the overall efficiency, size, and height of power conversion electronics in a very significant manner. In particular, the efficiency of the magnetic elements is of great value for the power converter designer.

A common problem in the design of a high-frequency magnetic component with an air gap is how the fringing field affects the high-frequency winding losses and how to configure the windings to minimize the effect of the fringing field of the air gap. A number of authors have addressed the problem of fringing field losses at high frequencies [1]–[9]. Most of the previous finite-element work [1]–[5] relates to multiple, discretely distributed air gaps as compared to a single lumped gap. It has been shown that distributing the gap along the magnetic path reduces winding loss, as compared to the loss in the case of a single lumped gap. Also, the emphasis in these works has been on the planar magnetics [2]–[5]. Two previous analytic works have also considered the problem of fringing field losses using 2-D solutions of electromagnetic equations [6], [7]. However, these solutions remain fairly complicated to use, one requiring numerical integrations while the other requires an iterative procedure. Furthermore, the solutions are provided only for the net fields, which include fringing fields, self fields, and proximity fields, and net losses and effects of fringing fields separately cannot be clearly discerned. Other related work includes the calculation of total energy and inductance [8], [9].

Thus, there is a need to derive simple analytic formulas that can be used to calculate fringing fields and the associated high-frequency winding losses. These formulas can be used to quickly evaluate the effect of fringing field on the winding designs, especially if there are a number of candidate designs being considered.

Another important motivation for this paper is that the current understanding about the fringing field and its effect on the winding loss is not very accurate (even qualitatively) and important questions remain open. For example, the question of how far away from the edge of the gap the fringing field remains important, is still not settled.

In this paper, by using a scalar potential approach, we have derived two simple formulas for the fringing fields. The geometry and coordinate system used in that paper is shown in Fig. 1. The two derived formulas for the $x$ and $y$ components of the fringing field $H$ are

$$\boxed{H_x(x,y) = \frac{H_g}{2\pi} \ln\left[\frac{x^2+(y-l_g)^2}{x^2+(y+l_g)^2}\right]} \tag{I.1}$$

and

$$\boxed{H_y(x,y) = -\frac{H_g}{\pi}\left\{\tan^{-1}\left[\frac{2xl_g}{x^2+y^2-l_g^2}\right] + m\pi\right\}} \tag{I.2}$$

where $m = 0$ if $x^2 + y^2 > l_g^2$ and $m = 1$ if $x^2 + y^2 < l_g^2$. $l_g$ is half of the total gap length. $H_g = 0.9NI/2l_g$. Further, we provide numerical (FEM) validation for these formulas. In addition, we address the issue of high-frequency fringing field loss by the use of the following well-known formula for high frequency eddy-current loss per unit length for a thin rectangular conductor [10]:

$$\boxed{P = \frac{1}{6\rho}(\pi\mu_o H_\perp f)^2 w^3 t} \tag{I.3}$$

where $\mu_o$ is the permeability of the free space, $H_\perp$ is the component of the fringing field, which is perpendicular to the long face of the conductor, $f$ is the frequency, $w$ is the width of the conductor, $t$ is the thickness of the conductor, and $\rho$ is the resistivity of the conductor material. The formula assumes that the skin effect is negligible.

Digital Object Identifier 10.1109/TMAG.2007.898908

Color versions of one or more of the figures in this paper are available online at http://ieeexplore.ieee.org.

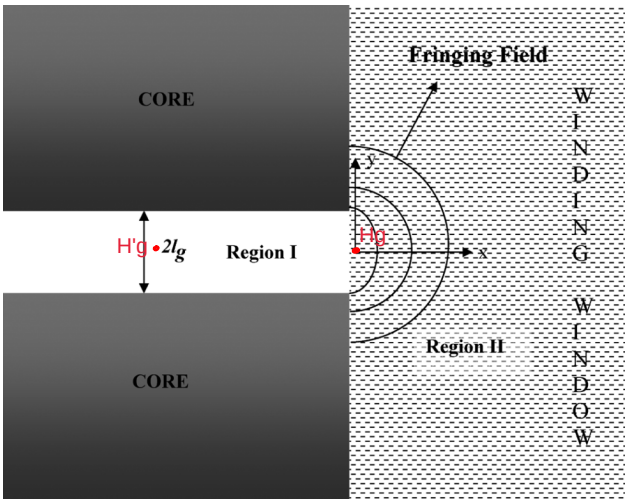


Fig. 1. Geometry for the air-gap and the coordinate system used in the paper.

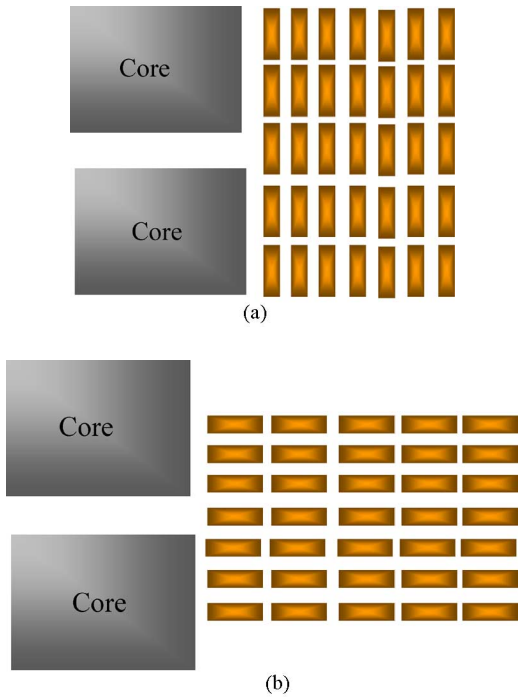


Fig. 2. (a) Barrel winding arrangement. (b) Flat (planar) winding arrangement.

Two winding arrangements of rectangular conductors are considered: 1) barrel wound [Fig. 2(a)] and 2) flat wound [Fig. 2(b)]. For barrel wound magnetic components, the width $w$ is along the $y$-axis and $H_\perp$ is equal to $H_x$, as given by (I.1) and evaluated at the center of the conductor for which loss is being calculated. Similarly, for flat wound magnetic components, the width $w$ is along the $x$-axis and $H_\perp$ should be taken to be $H_y$ of (I.2) evaluated at the center of the flat wound conductor for which the loss is to be calculated.

## II. Scalar Potential

There are several methods of calculating the magnetic field of a gap. Here, we use a scalar potential and separation of variables approach to obtain an exact expression for this scalar potential. We consider the region in and around the gap as a source-free region, which implies that self and proximity fields are negligible. This assumption has been verified using finite-element simulations both for the inductor and transformer cases. Then a scalar potential $\Phi(x,y)$ can be defined which satisfies the Laplace equation [11], [12] and is related to the magnetic field $H$ by

$$H = -\nabla\Phi(x,y). \tag{II.1}$$

The coordinates and the geometry are defined in Fig. 1. Here, $H_g$ is the magnetic field at the center edge of the gap ($x = 0$, $y = 0$). It is assumed that the gap is infinitely deep. This assumption is valid if the gap length is small compared to the dimension of the core. We also assume that the core pieces near the gap are equipotential. This assumption implies large permeability of the core material, which usually is a very good assumption. The scale of $H_g$ is set by the field at the center of the gap $H_g'$, which is given by

$$H_g' = \frac{NI}{2l_g + l_m/\mu} \cong \frac{NI}{2l_g} \tag{II.2}$$

where $NI$ is the driving amperes-turns, $2l_g$ is the gap length, $\mu$ is the permeability of the core material, and $l_m$ is the magnetic path length in the core. A large permeability is assumed. The exact relationship between $H_g$ and $H_g'$ can be determined by a magnetostatic finite-element calculation. However, for most inductor and transformer applications, the gap length is very small compared to the width of the core piece and it can be shown using finite-element simulation that

$$H_g \cong 0.9H_g' = 0.9\frac{NI}{2l_g}. \tag{II.3}$$

See Fig. 3 for a finite-element example.

In region I, the potential can be expanded as

$$\Phi(x,y) = \sum_{n=1}^{\infty} a_n \sin(n\pi y/l_g) e^{\frac{n\pi x}{l_g}} + \frac{H_g y}{2} \quad x<0,\ 0<y<lg. \tag{II.4}$$

In the region of primary concern, region II, the potential is given by

$$\Phi(x,y) = \int_0^{\infty} b(p)\sin(py)e^{-px}dp \quad x>0. \tag{II.5}$$

The field $H_g$ in (II.4) is given by (II.3). The constants $a_n$ and $b(p)$ are determined by matching the potential and the derivative at $x = 0$. Matching the potential at $x = 0$

$$\int_0^{\infty} b(p)\sin(py)dp = \begin{cases} \sum_{n=1}^{\infty} a_n \sin(n\pi y/l_g) & \\ \quad +H_g/l_g & 0 < y < l_g \\ H_g l_g & l_g < y < \infty. \end{cases} \tag{II.6}$$

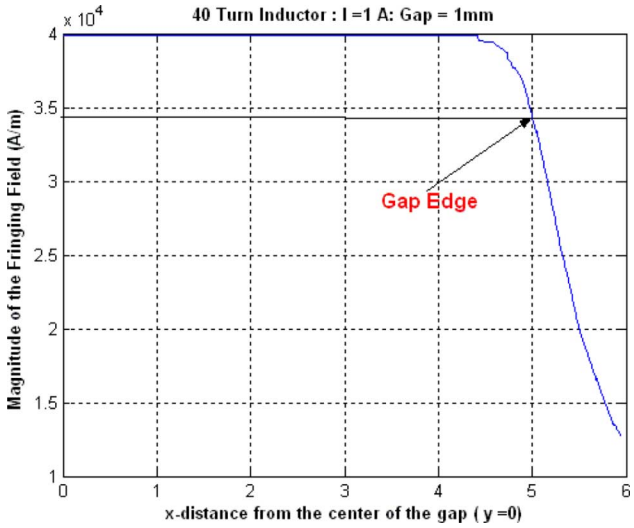


Fig. 3. Example of finite-element result showing the value of $H_g$ at the edge of the gap and the field value deep inside the gap.

Similarly matching the normal derivative at $x = 0$, we get

$$-\int_0^\infty b(p)\sin(py)dp = \sum_{n=1}^{\infty} a_n \sin(n\pi y/l_g)(n\pi/l_g) \quad 0<y<lg. \tag{II.7}$$

These two sets of equations can be solved for the coefficients $a_n$ and $b(p)$ by use of Fourier transforms. First, an equation for $b(p)$ is obtained by multiplying (II.6) with $\sin(py)$ and integrating over $y$. The left-hand side simplifies due to the orthogonality of the sine functions and only one $b(p)$ remains on the left-hand side. Similarly, an equation for the coefficients $a_n$ is obtained by multiplying (II.7) with $\sin(m\pi y/l_g)$ and integrating over $y$. In this case, only one term on the right-hand side survives due to the orthogonality of sine functions and one obtains an equation for $a_n$. Thus, one ends up with two sets of simultaneous equations. If the integrals on the right-hand side of the equation resulting from (II.6) and the integral on the left-hand side of the equation resulting from (II.7) are performed, then these two sets of equations can be solved for the two sets of coefficients $a_n$ and $b(p)$.

The resulting potential in the region of interest ($x > 0$) is given by

$$\Phi(x,y) = \frac{H_g}{\pi}\int_0^\infty dp e^{-px}\frac{\sin(pl_g)\sin(py)}{p^2} + \sum_{n=1}^{\infty} 2n(-1)^n a_n \int_0^\infty dp\cdot e^{-px}\frac{\sin(pl_g)\sin(py)}{p^2-(n\pi/l_g)^2} \tag{II.8}$$

where $a_n$ satisfy a set of algebraic equations

$$a_n = \frac{4}{\pi}(-1)^{n+1}\sum_{m=1}^{\infty} a_m(-1)^m C_{mn} + \frac{H_g B_n}{2} \tag{II.9}$$

where

$$B_n = \frac{(-2)}{n\pi}\left[ln(2n\pi) - Ci(2n\pi) + y\right] \tag{II.10}$$

and

$$C_{nm} = \begin{cases} (1/n\pi)\cdot Si(2n\pi) & m = n \\ \pi^2(n^2-m^2) \\ \quad \times[\ln(n/m) + Ci(2m\pi) - Ci(2n\pi)] & m \neq n \end{cases} \tag{II.11}$$

where $\gamma = 0.5772$ is the Euler's constant and $ln$ is the natural logarithmic function and

$$Ci(x_0) = \int_{x_0}^{\infty}\frac{\cos(x)}{x}dx \qquad Si(x0) = \int_0^{x_0}\frac{\sin(x)}{x}dx. \tag{II.12}$$

The coefficients $a_n$ are a decreasing function of $n$ (roughly $\sim l/n^2$). Thus, the first few terms make the dominant contribution. In Section V, it is shown that even just the first term gives a good approximation of the exact result.

## III. Fringing Fields

Differentiating the potential $\Phi$ with respect to $x$ and $y$, we obtain the $x$- and $y$-component of the magnetic field in the region $x > 0$

$$H_x(x,y) = \frac{Hg}{2\pi}\left\{\int_0^\infty dp(-\mathrm{p})\mathrm{e}^{-\mathrm{px}}\frac{\sin(pl_g)\sin(py)}{p^2} + \sum_{n=1}^{\infty} 2n(-1)^{\mathrm{n}}\mathrm{a_n}\int_0^\infty dp(-\mathrm{p})\mathrm{e}^{-\mathrm{px}}\frac{\sin(pl_g)\sin(py)}{p^2-(n\pi/l_g)^2}\right\} \tag{III.1}$$

$$H_y(x,y) = \frac{Hg}{\pi}\left\{\int_0^\infty dp(\mathrm{p})\mathrm{e}^{-\mathrm{px}}\frac{\sin(pl_g)\cos(py)}{p^2} + \sum_{n=1}^{\infty} 2n(-1)^{\mathrm{n}}\mathrm{a_n}\int_0^\infty dp(\mathrm{p})\mathrm{e}^{-\mathrm{px}}\frac{\sin(pl_g)\cos(py)}{p^2-(n\pi/l_g)^2}\right\}. \tag{III.2}$$

As a first approximation, we keep only the first terms in (III.1) and (III.2) to obtain

$$H_x(x,y) = \frac{Hg}{\pi}\int_0^\infty dp(-p)e^{-px}\frac{\sin(pl_g)\sin(py)}{p^2} \tag{III.3}$$

$$H_y(x,y) = \frac{Hg}{\pi}\int_0^\infty dp(p)e^{-px}\frac{\sin(pl_g)\cos(py)}{p^2}. \tag{III.4}$$

Integrations in the above two equations yield the approximate analytic result [13]

$$H_x(x,y) = -\frac{Hg}{2\pi}ln\left[\frac{x^2+(y-l_g)^2}{x^2+(y+l_g)^2}\right] \tag{III.5}$$

$$H_y(x,y) = -\frac{Hg}{\pi}\left\{\tan^{-1}\left[\frac{2xl_g}{x^2+y^2-l_g^2}\right]+m\pi\right\} \tag{III.6}$$

where $m = 0$ if $x^2 + y^2 > l_g^2$ and $m = 1$ if $x^2 + y^2 < l_g^2$.

Verifications for (III.5) and (III.6) are provided in Section V. These two approximate results can then be used to calculate the high-frequency conductor losses. Depending on the winding

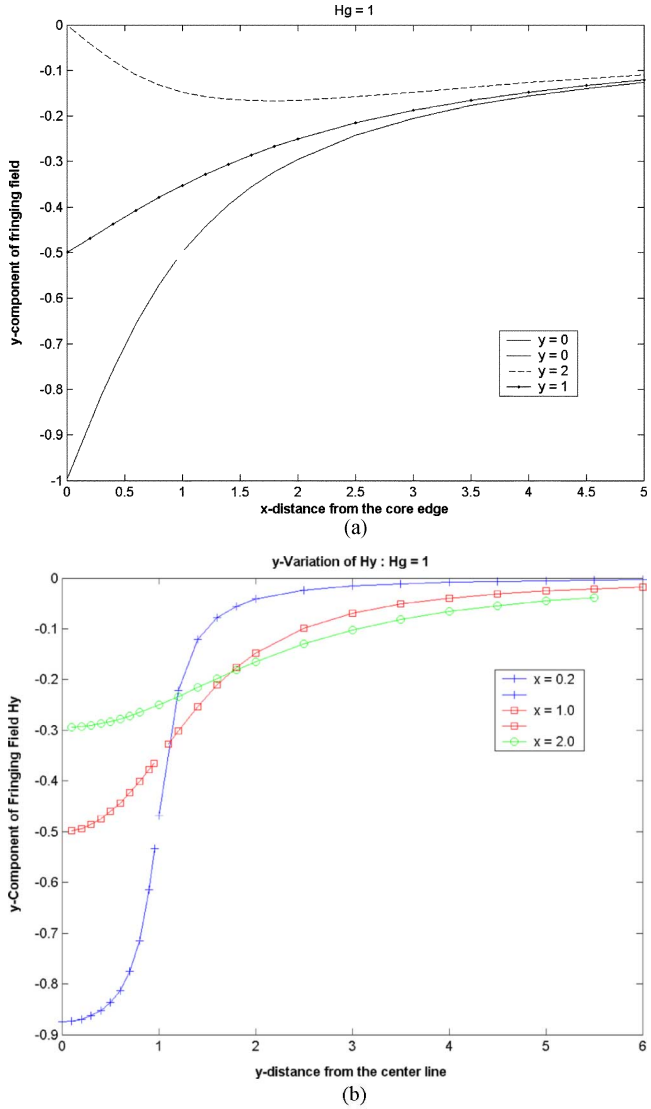


Fig. 4. (a) Variation of the $y$-component of the fringing field $H_y$ with the $x$ (horizontal) distance from the edge of the core. Gap length $= 2l_g = 2$. (b) Variation of the $y$-component of the fringing field $H_y$ with $y$ (vertical) distance from the center line with $x$ as a parameter. Gap length $= 2l_g = 2$.

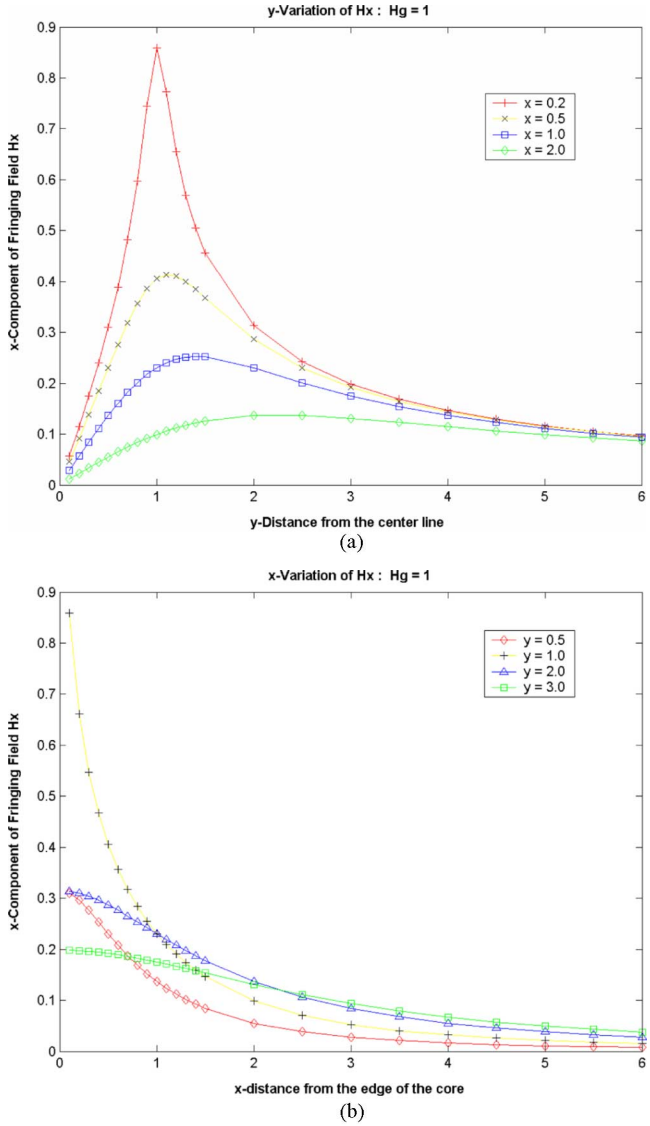


Fig. 5. (a) Variation of the $x$-component of the fringing field $H_x$ with the y(vertical) distance from the central line with $x$ as a parameter. $H_g = 1$; Gap length $= 2l_g = 2$. (b) Variation of $x$-component of the fringing field $H_x$ with the $x$ (horizontal) distance from the edge of the core for fixed values of $y$. $H_g = 1$; gap length $= 2l_g = 2$.

configuration ("flat" versus "barrel"), either the $x$-component or the $y$-component is important [see Fig. 2(a) and (b)].

## IV. Field Distribution

Fig. 4(a) shows the variation of the $y$-component of the field $H_y$ with the horizontal distance $x$ from the edge of the core for four different values of $y$. These fields have been obtained by setting $H_g = 1$. It is also assumed that $l_g = 1$. We remind the reader that the total gap length is equal to $2l_g$. Generally, the field falls off substantially within one gap length distance $(2l_g)$ from the edge of the core. However, it is important to note that the field component remains substantially higher than other fields (self and proximity fields) in the problem, even after 10 gap length distance. We have confirmed this by using finite-element modeling. Thus, the fringing cannot be neglected even at such large distances from the core and may determine the overall loss in a winding conductor at such distances. Another interesting feature to note from Fig. 4(a) is that for $y > 1$, the initial value of $H_y$ for $x = 0$ must be zero because of the boundary condition imposed by the large permeability of the core.

Similarly, Fig. 4(b) shows the variation of the $y$-component of the field $H_y$ with the vertical distance $y$ with $x$ as a parameter. First thing we note is that for small $x$, there is a sharp drop in the value of the field as we approach the core corner of the core $(y = 1)$, which is again due to the boundary condition, that at the surface of the core the field must be perpendicular to the surface of the core. For more important cases of practical interest, where there is substantial insulation separating the core from the windings, $x$ is usually $>1$. For such cases, we see from Fig. 4(b) the drop in the value of the field is much more gradual.

Fig. 5(a) shows the variation of the $x$-component of the fringing field $H_x$ with the $y$ (vertical) distance from the central line for various values of $x$, the horizontal distance from the core. The most outstanding feature with regards to $H_x$ is that its value peaks near the corner of the gap $(y \sim 1.0)$, in sharp contrast to $H_y$, which peaks along the central line $(y \sim 0)$. The

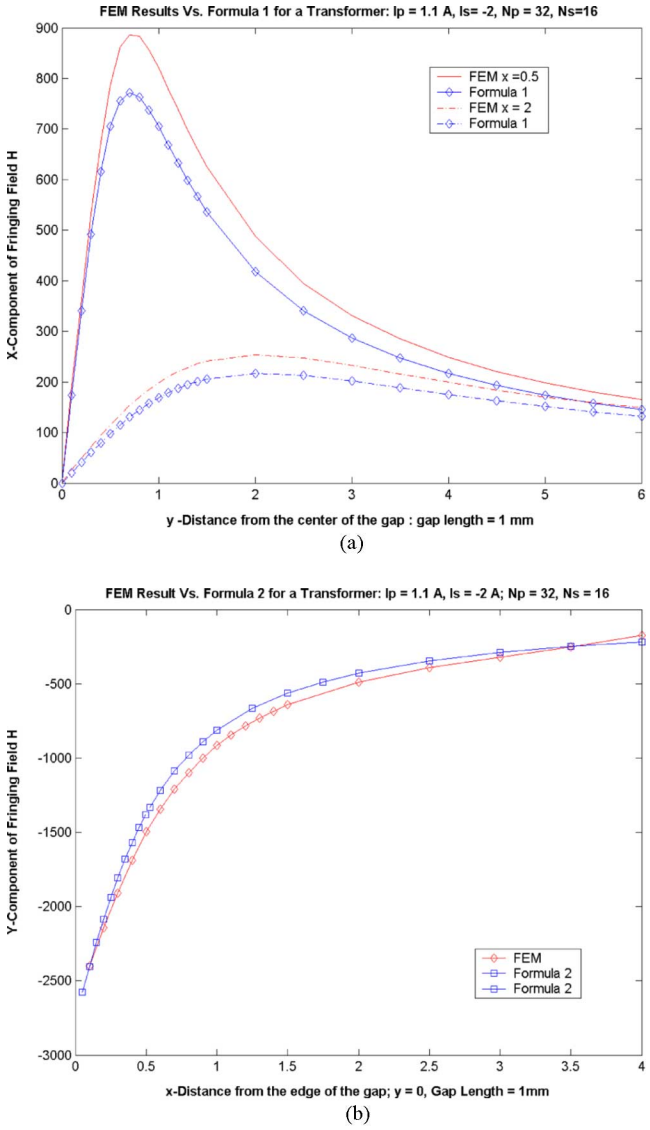


Fig. 6. (a) Comparison of the calculated fringing field component $H_x$ of a transformer with the finite-element simulation. (b) Comparison of the calculated fringing field component $H_y$ of a transformer with the finite-element simulation.

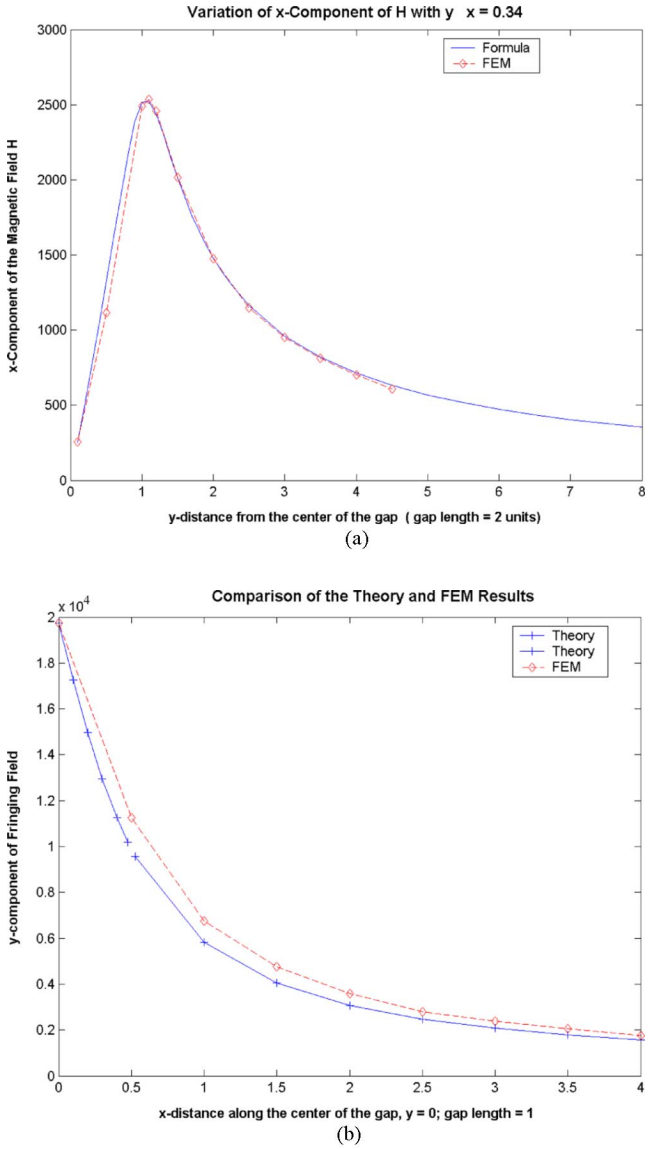


Fig. 7. (a) Comparison of the calculated fringing field component $H_x$ of a inductor with the finite-element simulation. (b) Comparison of the calculated fringing field component $H_y$ of a inductor with the finite-element simulation results.

symmetry of the model forces $H_x$ to be zero or near zero along the central line. This feature has not been fully recognized in the past. In particular, it indicates that for barrel type windings, shown in Fig. 2(b), the maximum fringing field loss would occur not along the central line but near the corner of the gap.

Fig. 5(b) shows the variation of $H_x$ with $x$ for fixed values of $y$. Once again we see that the peak of the initial value of $H_x$ occurs near $y \sim 1$ (near the corner). However, another interesting feature, which is apparent from Fig. 4(b), is that the curves, which start out high, also show steeper decline as the value of $x$ is increased. In fact some of the curves that start out low in value can have larger values as $x$ is increased.

## V. Numerical Validation for Fields

In order to validate the fringing fields' formulas (I.1) and (I.2), we have performed extensive numerical (FEM) calculations and have found good agreement between the numerical results and the formulas both for transformers and inductors having an air gap.

In Fig. 6(a) and (b), we show the comparison of finite-element simulation with the calculations using (I.1) and (I.2) for the $x$ and $y$ components of the fringing field in the case of a gapped transformer. The transformer had a gap length of 1 mm, a turn's ratio of 2:1, and driving current of one ampere. The number of primary turns was 32 and the primary and secondary were inter-leaved. As is clear from these graphs, generally the agreement between finite-element simulation results and the results obtained using formulas is very good. In particular, the form of variation of $H_x$ and $H_y$ is described exactly. In addition, there is excellent agreement between the magnitudes calculated, using (2) for $H_y$ and the finite-element results. In the case of $H_x$, the agreement is not as good with a difference of about 10%–15%. This may be caused by the sharp corner of the model, which

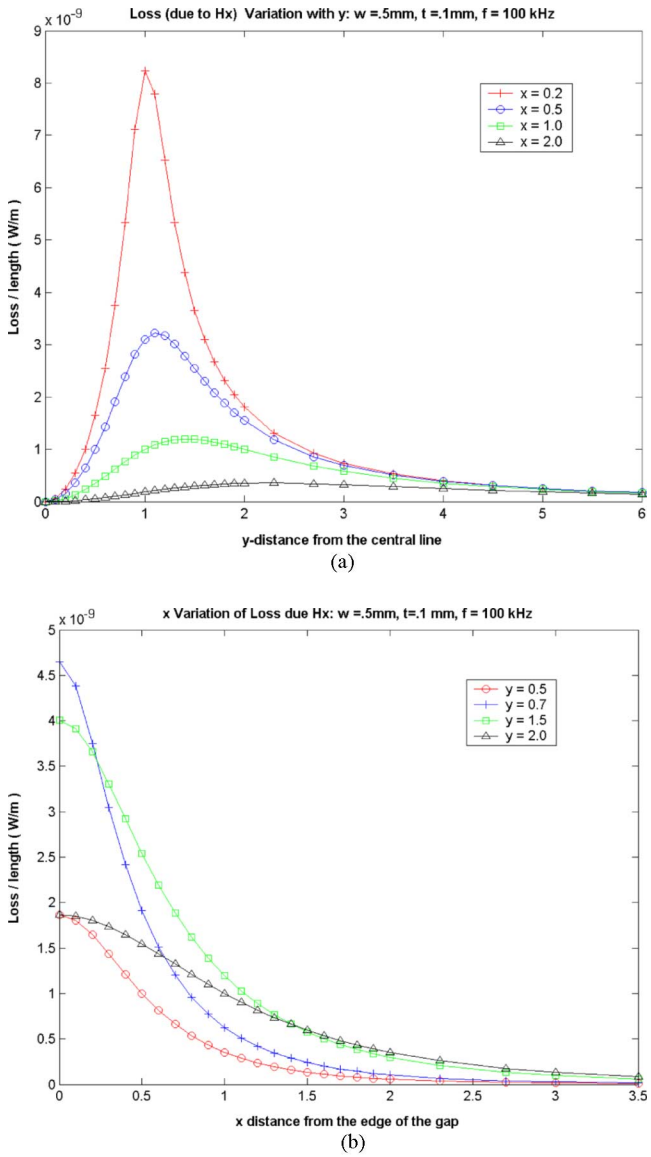


Fig. 8. (a) Variation of loss due to $H_x$ (barrel wound) with $y$ for fixed values of $x$. (b) Variation of loss due to $H_x$ (barrel wound) with $x$ for fixed values of $y$.

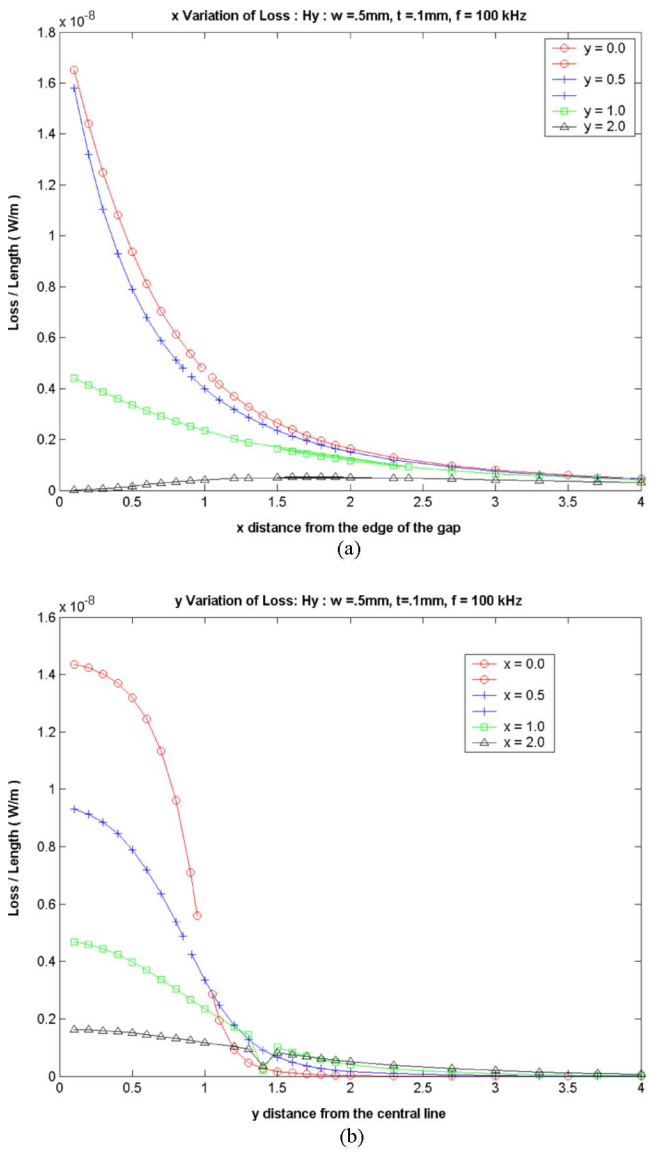


Fig. 9. (a) Variation of loss due to $H_y$ (flat wound winding) with x for fixed values of $y$. (b) Variation of loss due $H_y$ (flat wound winding) with $y$ for fixed values of $x$.

produces large variations in the fields around the corners of the gaps.

Fig. 7(a) and (b) shows a similar comparison in the case of an inductor. The inductor had 24 turns, a gap length of 1 mm, and a driving current of one ampere. Once again the agreement between calculated results for $H_x$ and $H_y$ and finite-element simulation is excellent.

## VI. Loss Distribution

Next we consider high frequency winding loss of thin rectangular winding conductors by employing the well-known formula (I.3). We first consider loss due to the $H_x$ distribution, which is the more important component of the field for the barrel wound windings, shown in Fig. 2(a). Fig. 8(a) shows the variation of the loss due to this component as a function of $y$ for fixed values of $y$. For these figures, the following values are used in (V.8): $w = 0.5$ mm, $t = 0.1$ mm, $f = 100$ kHz, $1/\rho = 5.8 \times 10^7$ mho/m, and $\mu_o = 4\pi \times 10^{-7}$. The most important feature, which is somewhat surprising, is that the loss shows a maximum near $y \sim 1$ (near the corner) instead of $y \sim 0$ (near the central line). This is because the field component $H_x$ shows a maximum around $y \sim 1$ as shown in Fig. 5(a). Similarly, Fig. 8(b) shows the same loss as a function of $x$ for fixed values of $y$.

Next, we consider the loss for the flat wound winding for which the $y$ component of the field $H_y$ is more important. Fig. 9(a) shows the loss as a function of $x$ for fixed values of $y$. We see that the initial value of loss is largest for the smaller values of $y$ (near the central line). However, the drop in the values as $x$ is increased is also steeper for these values of $x$. For larger values of $x$, all curves approach roughly the same value irrespective of the value of $y$, indicating for some distance from the core losses would be somewhat independent of the vertical position. Similarly, Fig. 9(b) shows the variation of this loss with $y$ for fixed values of $x$. Once again we see a similar

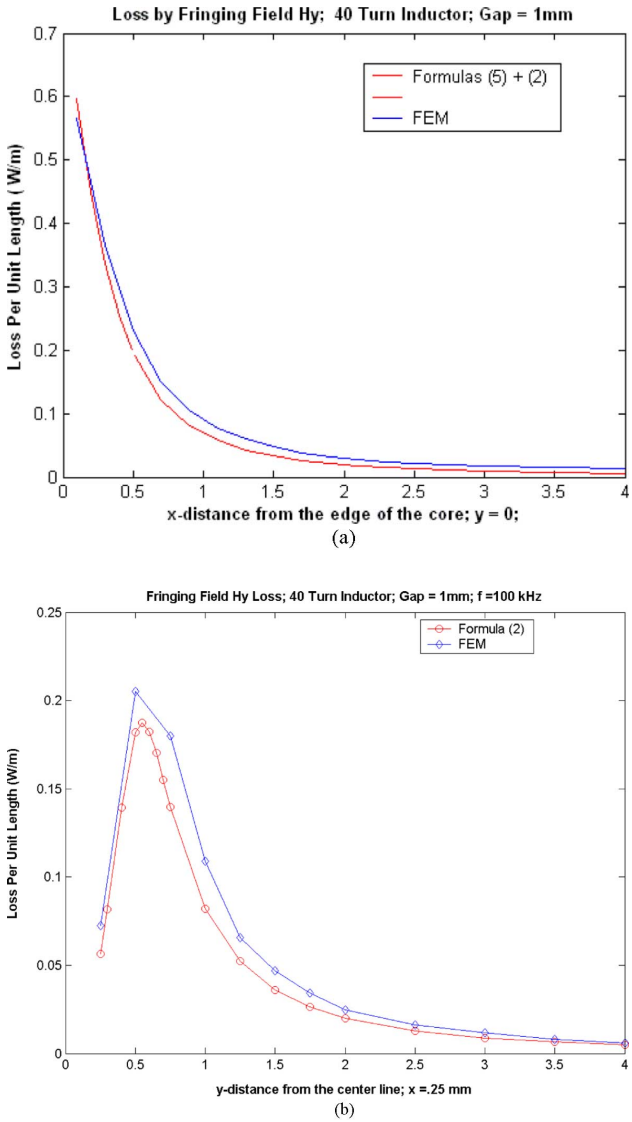


Fig. 10. High-frequency loss per unit length of a conductor with aspect ratio of 4:1 due to (a) $y$-component and (b)$x$-component of the fringing field.

variation, where the initial values of the loss start high near the core edge $(x < 1)$ but shows a much steeper decline in the value as $y$ is increased.

## VII. Numerical Validation for Loss

Fig. 10(a) and (b) shows the comparison of the theoretical computational results of fringing field high frequency loss using (I.3), and either (1) or (2) with finite-element simulation results. The results are shown for a 40-turn inductor only but the results for a gapped transformer are similar. The exciting current is one ampere and the gap length is 1 mm. The frequency was chosen to be 100 kHz. The conductor for which loss is calculated has an aspect ratio of 4:1 and is made of copper. For Fig. 10(a), the results are shown along a horizontal line with $y = 0$. This line was chosen because $Hy$ is the largest along this line. The conductor was placed so that its long face was horizontal. For Fig. 9(b), the conductor was placed along a vertical line with $x = 0.25$ mm with its face vertical.

It is clear from Fig. 10(a) and (b) that there is general agreement between the finite-element results and the results obtained by using (I.3) for both the $x$ and $y$ component of the fringing field. A somewhat larger difference in the case of Fig. 10(b) may be due to the sharp corner, which makes it somewhat hard to satisfy boundary conditions in the finite-element algorithms.

## VIII. Conclusion

We have derived two simple formulas for the calculation of fringing field components. We have shown that these formulas can be used for calculating high-frequency fringing field loss for thin rectangular conductors. Both the field formulas and loss calculations have been validated numerically using finite-element analysis. The formulas for fringing fields may also be applicable to electrical machines such as motors and generators where air gaps can determine the field distribution, the power converted (from electrical to mechanical or vice versa), as well as the losses.

Also to be noted is that even though we have discussed the loss calculations only for thin rectangular conductors and is directly applicable to thin film [14]–[16], thick film [17], printed circuit board and flex circuit [18] windings, the qualitative conclusions regarding the variation of the loss with the position of the conductors also apply to other conductor shapes as round wires and thick rectangular conductors. However, in many cases more exact formulas would be needed for shapes other than thin rectangular conductors. In particular, the formula for the fringing field loss for a round conductor would be needed. Also, the formula for rectangular conductors with an aspect ratio close to 1:1 is needed. Dealing with both of these conductor shapes requires the simultaneous incorporation of both $x$ and $y$ components of the fringing field in the loss calculation. This can be done using the principle of superposition. We intend to develop such formulas in a near future publication.

While it is true that the fringing field, if present, is overwhelmingly dominant over the self and proximity effect field (generally speaking), some of the winding conductors may be placed far away from the air gap. In such a case the fringing field may have decayed enough to become comparable in magnitude to the self and proximity fields. In this situation, one must use all three fields in the calculation of the winding loss. Once again, the principle of superposition can be used. A future publication would address the problem of incorporating self and proximity fields in the analysis of fringing field loss.

The current paper also neglects skin effect. Inclusion of this effect may pose a formidable challenge and is beyond the scope of the present work. However, if the fringing field by itself does vary appreciably along the width of the conductor, a rough treatment suggests that the skin effect may be incorporated, approximately, by modifying (I.3) as follows:

$$\boxed{P = \tfrac{1}{6\rho}(\mu_o H_\perp f)^2 w^3 t \times F(\zeta)} \qquad \text{(VIII.1)}$$

where the function $F(\zeta)$ is given by

$$F(\zeta) = \frac{3}{\zeta}\frac{\sinh\zeta - \sin\zeta}{\cosh\zeta - \cos\zeta} \qquad \text{(VIII.2)}$$

and where $\zeta = w/\delta$ and $\delta$ is the skin depth. A future publication will provide a fuller description of the derivation of (VIII.1) and finite-element simulation verification.

Although, in this paper, we have only considered high frequency winding losses due to the fringing fields, the fringing field formulas (I.1) and (I.2) derived here may also be used for calculating laminations core losses of low frequencies ($\sim$50 Hz) reactors, where split laminations are used [19], [20]. A future publication will explore these types of core losses in greater detail.

## REFERENCES


[1] J. Hu and C. R. Sullivan, "Optimization of shapes for round-wire high-frequency gapped-inductor windings," in *Conf. Record. IEEE Industry Applications Conf.*, 1998, pp. 907–911.

[2] J. Hu and C. R. Sullivan, "AC resistance of planar power inductors and the quasidistributed gap technique," *IEEE Trans. Power Electron.*, vol. 16, no. 4, pp. 558–567, Jul. 2001.

[3] K. D. T. Ngo and M. H. Kuo, "Effects of air gaps on winding loss in high-frequency planar magnetics," in *19th Power Electronic Specialist Conf.*, 1988, pp. 1112–1119.

[4] N. H. Kurkut and D. M. Divan, "Optimal air-gap design in high frequency foil windings," *IEEE Trans. Power Electronics*, vol. 13, no. 5, pp. 942–949, Sep. 1998.

[5] L. Ye, G. R. Skutt, R. Wolf, and F. C. Lee, "Improved winding design for planar inductors," in *Proc. IEEE Power Electronics Specialists Conf.*, 1997, vol. 2, pp. 1561–1567.

[6] M. Albach and H. Robmanith, "The influence of air gap size and winding position on the proximity losses in high frequency transformers," in *Conf. Rec. IEEE Power Electronics Specialists Conf.*, 2001, pp. 1485–1490.

[7] P. Wallmeirer, N. Frohleke, and H. Grotstollen, "Improved analytical modelling of conductive losses in gapped high frequency inductors," in *Conf. Record. IEEE Industry Applications Conf.*, 1998, pp. 913–920.

[8] L. M. Escribano, R. Prieto, J. A. Oliver, J. A. Cobos, and J. Uceda, "New modeling strategy for the fringing energy in magnetic components with air gap," in *Proc. IEEE Power Electronics Specialists Conf.*, 2002, pp. 144–150.

[9] A. Balakrishman, W. T. Jones, and T. G. Wilson, "Air gap reluctance and inductance calculations using a Schwarz-Christoffel transformation," in *Proc. IEEE Power Electronics Specialist Conf.*, 1995, vol. 2, pp. 1050–1056.

[10] E. C. Snelling, *Soft Ferrites: Properties and Applications*, 2nd ed. London, U.K.: Butterworth, 1988.

[11] J. D. Jackson, *Classical Electrodynamics*, 3rd ed. New York: Wiley, 1999.

[12] P. Lorain and D. Corson, *Electromagnetic Fields and Waves*. San Francisco, CA: Freeman, 1970.

[13] I. S. Gradshteyn and I. M. Ryzhik, *Table of Integrals, Series, and Products*. New York: Academic, 1980.

[14] L. Daniel, C. R. Sullivan, and S. R. Sanders, "Design of microfabricated inductors," *IEEE Trans. Power Electron.*, vol. 14, no. 4, pp. 709–723, Jul. 1999.

[15] T. Sato, H. Tomita, A. Sawabe, T. Inoue, T. Mizoguchi, and M. Sahashi, "A magnetic thin film inductor and its application to a MHz switching dc-dc converter," *IEEE Trans. Magn.*, vol. 30, no. 2, pp. 217–223, Mar. 1994.

[16] W. A. Roshen and D. E. Turcotte, "Planar inductors on magnetic substrates," *IEEE Trans. Magn.*, vol. 24, no. 6, pp. 3213–3216, Nov. 1988.

[17] F. Gradzki and F. Lee, "Design of high-frequency hybrid power transformer," in *Proc. 6th Annual Power Electronics Seminar, VPEC*, 1988, pp. 319–326.

[18] W. Roshen *et al.*, "High frequency, high density MHz magnetic components for a low profile converter," in *1992 IEEE Applied Power Electronics Conf. Rec.*, 1992, pp. 674–683.

[19] S. Nagawa, M. Kuwata, T. Nakau, D. Miyagi, and N. Takahashi, "Study of modeling method of lamination of reactor core," *IEEE Trans. Magn.*, vol. 42, no. 4, pp. 1455–1458, Apr. 2006.

[20] S. Nogawa, M. Kuwata, D. Miyagu, H. Tounai, T. Nakau, and N. Takahashi, "Study of eddy current loss reduction of slit in reactor core," *IEEE Trans. Magn.*, vol. 41, no. 9, pp. 2024–2027, Sep. 2005.


Manuscript received December 28, 2006; revised April 29, 2007. Corresponding author: W. A. Roshen (e-mail: wroshen@msn.com).